Isotope yields from central ^{112,124}Sn + ^{112,124}Sn collisions: Dynamical emission?

T. X. Liu, M. J. van Goethem, X. D. Liu, W. G. Lynch, R. Shomin, W. P. Tan, M. B. Tsang, G. Verde, A. Wagner,* H. F. Xi,† and H. S. Xu
National Superconducting Cyclotron Laboratory and Department of Physics and Astronomy, Michigan State University, East Lansing, Michigan 48824, USA

M. Colonna and M. Di Toro
Laboratorio Nazionale del Sud, Via S. Sofia 44, I-95123 Catania, Italy and University of Catania, I-95123 Catania, Italy

M. Zielinska-Pfabe
Department of Physics, Smith College, Northampton, Massachusetts 01063, USA

H. H. Wolter
Ludwig-Maximilians-Universität, München, Germany

L. Beaulieu, B. Davin, Y. Larochelle, T. Lefort, R. T. de Souza, R. Yanez, and V. E. Viola
Department of Chemistry and IUCF, Indiana University, Bloomington, Indiana 47405, USA

R. J. Charity and L. G. Sobotka
Department of Chemistry, Washington University, St. Louis, Missouri 63130, USA
(Received 20 August 2002; revised manuscript received 5 June 2003; published 15 January 2004)

Isotopic yields for light particles and intermediate mass fragments have been measured for central ^{112}Sn + ^{112}Sn, ^{112}Sn + ^{124}Sn, ^{124}Sn + ^{112}Sn, and ^{124}Sn + ^{124}Sn collisions at $E/A = 50$ MeV and compared with predictions of stochastic mean field calculations. These calculations predict a sensitivity of the isotopic distributions to the density dependence of the asymmetry term of the nuclear equation of state. However, the secondary decay of the excited fragments modifies significantly the primary isotopic distributions and these modifications are rather sensitive to theoretical uncertainties in the excitation energies of the hot fragments. The predicted final isotope distributions are narrower than the experimental data and the sensitivity of the predicted yields to the density dependence of the asymmetry term is reduced.

DOI: 10.1103/PhysRevC.69.014603 PACS number(s): 24.10.−i, 25.70.−z

I. INTRODUCTION

The density dependence of the asymmetry term in the nuclear equation of state (EOS) is an important but poorly constrained property of nuclear matter [1–3]. Nuclear structure data provide few constraints on the density dependence of the asymmetry term [3]. On the other hand, the asymmetry term and its density dependence govern the density, radius, and proton fraction of neutron stars [2], and provide strong motivations for theoretical and experimental investigations of these issues. Recently, a number of calculations have tried to identify experimental observables, which can provide constraints on the density dependence of the asymmetry term [4–7].

In this paper, we focus on sensitivities that have been predicted for observables in energetic central nucleus collisions [4–7]. At incident energies of 50*A* MeV and above, the central density in such collisions initially increases as the projectile and target nuclei overlap and then decreases as the system collectively expands [8,9]. Previous investigations have shown that excited systems produced in such collisions undergo bulk multifragmentation characterized by a short breakup time scale 100 fm/*c* [10–13] and final states containing more than four fragments of charge $Z > 2$ [14,15].

For heavy systems in which the neutron density exceeds the proton density, the asymmetry term is repulsive for neutrons and attractive for protons. The asymmetry term therefore enhances the dynamical emission of neutrons relative to protons in such collisions; the degree of enhancement reflects the magnitude of the asymmetry term and its density dependence [4–7]. The difference between neutron and proton emission rates in such collisions can either be probed by direct measurements of preequilibrium neutron and proton spectra or by examining the isotopic composition of the bound fragments that remain after emission [4–7]. In this paper, we will concentrate on the fragment observables.

Fragment observables for these reactions have been described successfully via either statistical [16–19] or dynamical [20,21] models. To investigate the dependence of such observables on the density dependence of the asymmetry term, it is necessary to calculate the relative emission of neutrons and protons and assess the change in the isotopic

*Present address: Institut für Kern- und Hadronenphysik, Forschungszentrum Rossendorf, D-01314 Dresden, Germany.

†Present address: Benton Associate, Toronto, Ontario, Canada.

composition in the prefragment during the expansion stage prior to the multifragment breakup [4]. Within the context of a hybrid model, this preequilibrium emission was calculated in Ref. [22] using a Boltzmann-Uehling-Uhlenbeck (BUU) equation model of Ref. [4] and the subsequent fragmentation was explored using the equilibrium statistical multifragmentation model (SMM) of Ref. [23]. In a second approach [24], the expansion and multifragmentation of the system was calculated by a statistical rate equation approach for surface emission called the Expanding Emitting Source (EES) model of Ref. [16]. Both of these calculations predicted that the final isotopic composition of observed fragments should be sensitive to the density dependence of the asymmetry term.

The predicted sensitivities for the surface emission in the EES calculations and for the bulk emission in the hybrid BUU-SMM calculations, however, are completely opposite [22,24]. For calculations using an asymmetry term with softer density dependence, the EES approach predicts preferential surface emission of more neutron-rich fragments while the BUU-SMM approach predicts preferential bulk emission of more isospin symmetric fragments. These differences stem from different model assumptions in these two approaches about the density distribution of the system at the time of fragment production. In the EES approach, the fragments are emitted at normal density along with the protons and neutrons from a residue, which is at subnuclear density. In the BUU-SMM approach, the fragments originate from the bulk disintegration of the residue itself.

In this paper, we investigate how the isospin transport and dynamics is related to the asymmetry term within the dynamical stochastic mean field (SMF) theory approach wherein the evolution of the density and nuclear mean field is calculated self-consistently [7,25]. In previous publications, stochastic mean field theory predictions for the influence of the asymmetry term on fragment production, collective flow, incomplete fusion, and binary collisions have been reported [26–28]. Here, we compare this model to isotopically resolved multifragmentation data measured in central ^{124}Sn+^{124}Sn and ^{112}Sn+^{112}Sn reactions at 50*A* MeV. These experimental multifragmentation data are presented in the following section. This is followed by a description of the SMF approach, which provides predictions for the dynamical production of highly excited fragments, and of the decay of these excited fragments via the MSU statistical decay code [29–31]. The paper concludes with a discussion of the comparison between data and theory and the issues that remain for future investigations.

II. THE EXPERIMENT

Central ^{112}Sn+^{112}Sn, ^{112}Sn+^{124}Sn, ^{124}Sn+^{112}Sn, and ^{124}Sn+^{124}Sn collisions were measured at the National Superconducting Cyclotron Laboratory at Michigan State University, using 5 mg/cm^2 ^{112}Sn and ^{124}Sn targets and 50-MeV-per-nucleon ^{112}Sn and ^{124}Sn beams. Isotopically resolved light particles and intermediate mass fragments with $3 \leqslant Z \leqslant 8$ were measured with the large area silicon strip detector array (LASSA) [32,33], an array consisting of nine telescopes, each comprised of one 65-μm and one 500-μm Si strip detector, followed by four 6-cm-thick CsI(Tl) detectors. The 50×50 mm^2 lateral dimensions of each LASSA telescope are divided by the strips of the second silicon detector into 256 (3×3 mm^2) square pixels, providing an angular resolution of about $\pm 0.43°$. The LASSA device was centered at a polar angle of $\theta_{lab} = 32°$ with respect to the beam axis, providing coverage at polar angles of $7° \leqslant \theta_{lab} \leqslant 58°$. At other angles, charged particles were detected in 188 plastic scintillator—CsI(Tl) phoswich detectors of the Miniball/Miniwall array [34], which subtended polar angles $7° \leqslant \theta_{lab} \leqslant 160°$. The Miniball/Miniwall array provided isotopic resolution for H and He nuclei and elemental resolution for intermediate mass fragments (IMF's) with $3 \leqslant Z \leqslant 20$.

The total charged-particle multiplicity detected in the two arrays was used for impact parameter determination. Central collisions, corresponding to a reduced impact parameter of $b/b_{max} \leqslant 0.2$ [35], were selected by a gate on the top 4% of the charged-particle multiplicity distribution. Here, b_{max} corresponds to a trigger threshold requirement of three charged particles detected in any of the 188 Miniball elements. From cross section measurements for such events, we estimate a value for $b_{max} = 7.3 \pm 0.4$ fm by neglecting fluctuations and assuming that multiplicity decreases monotonically with impact parameter. This would suggest that our impact parameter selection corresponds to $b \leqslant 1.5$ fm; however, multiplicity fluctuations at fixed impact parameter may extend the included range of impact parameters outward (up to $b \approx 3$ fm).

In the following we present isotopically resolved differential multiplicities for fragments emitted at center of mass angles of $70° \leqslant \theta_{\mathrm{c.m.}} \leqslant 110°$. At these angles, the coverage of the LASSA array is excellent; the only losses occurred for fragments emitted at very low energies $E/A < 0.2$ MeV in the center of mass, corresponding to small laboratory angles of $\theta_{lab} < 7°$.

This enabled accurate calculation of the detection efficiency for $70° \leqslant \theta_{\mathrm{c.m.}} \leqslant 110°$; the fragment spectra were fitted and the losses at low energies ($<2\%$) were estimated and corrected. The data presented below have been corrected for the losses below threshold, for inefficiencies in the solid angle coverage and for multiple hits in the detector telescopes. The acceptance of LASSA and the impact of this acceptance cut on the data are both illustrated in Fig. 1, where the efficiency corrected differential multiplicity $dM/dydp_\perp$ for ^{12}C fragments are shown. The cut $70° \leqslant \theta_{\mathrm{c.m.}} \leqslant 110°$ is indicated by the dashed lines in the figure. The measured differential multiplicities smoothly depend on the transverse momentum $p_\perp$ and rapidity y and are centered about the rapidity of the center of mass, consistent with emission from the participant source. They display no characteristic "Coulomb holes" near the projectile rapidity, expected from the Coulomb repulsion of ^{12}C fragments from projectile-like residues moving with velocities somewhat less than that of the projectile.

Figure 2 shows the measured average differential multiplicities of Li, Be, B, C, N, and O isotopes at $70° \leqslant \theta_{\mathrm{c.m.}} \leqslant 110°$. In this figure, the solid squares and circles show the ^{112}Sn+^{112}Sn and ^{124}Sn+^{124}Sn data, respectively. The isotopic yields of ^{112}Sn+^{124}Sn and ^{124}Sn+^{112}Sn are essentially

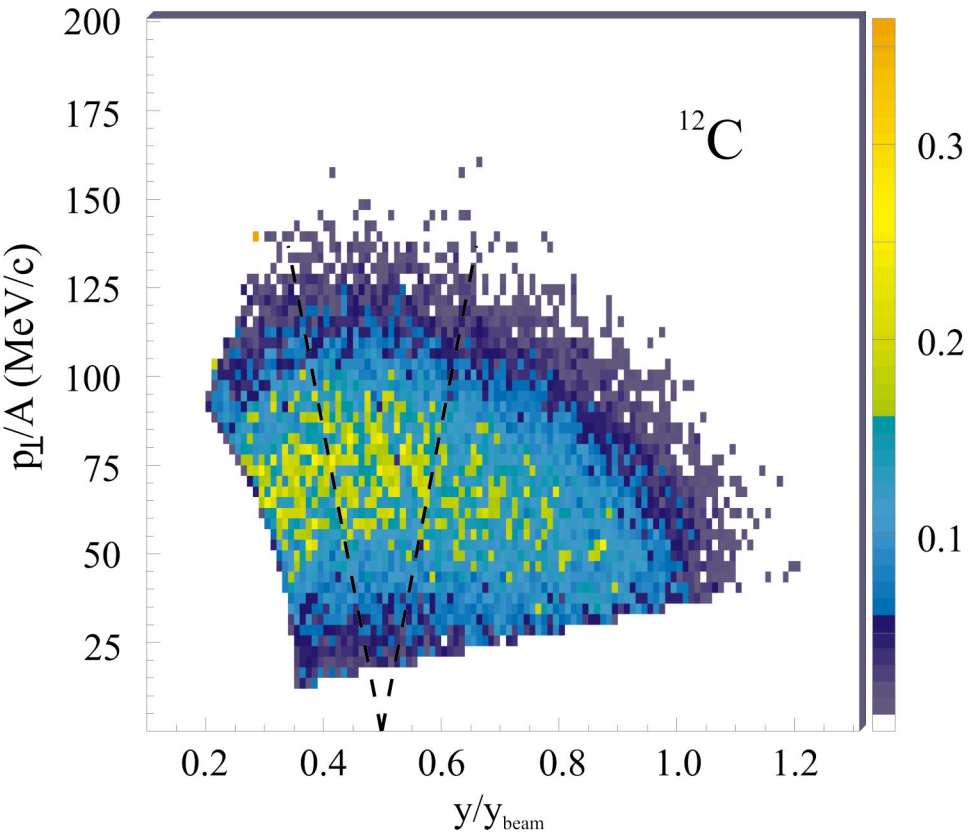

FIG. 1. (Color) Efficiency corrected differential multiplicity $dM/dydp_\perp$ for ^{12}C fragments. The cut $70° \leqslant \theta_{c.m.} \leqslant 110°$ is indicated by the dashed lines in the figure. The color scale in the right side of the figure indicates the relationship between the colors and the values for $dM/dydp_\perp$ in units of GeV/c^{-1}.

equal; they have been averaged and are shown by the open diamonds. The x axis, $N-Z$, corresponds to the neutron excess of the nuclides. The peaks of the distributions are typically located at isotopes with $N=Z+1$. The yields of the B and C isotopes are offset by a factor of 10 and the yields of the N and O isotopes are offset by a factor of 100 in the figure. As expected, more neutron-rich nuclide are produced by the neutron-rich system, ^{124}Sn+^{124}Sn, while the opposite is true for emission from the proton-rich isotope system, ^{112}Sn+^{112}Sn. The experimental results indicate that the multiplicities of IMF's are $\approx$10–20 % larger for the ^{124}Sn +^{124}Sn entrance channel than for the ^{112}Sn+^{112}Sn entrance channel, consistent with previous observations at an incident energy of 40 MeV per nucleon [36].

In general, the drop from the peak toward more proton-rich isotopes is rather steep especially for elements with even values of Z. The main differences between the isotope yields for the four different systems are observed in the tails of the isotope distributions, where it is greater than a factor of 4 for ^{20}O. Larger differences may be expected for even more exotic isotopes, but the background in the present measurement due to multiple hits in the LASSA telescopes does not allow for their accurate determination.

Recently, it has been shown [37] that the isotopic yields for systems produced at approximately the same excitation energy per nucleon or the same temperature satisfy an isoscaling relationship. Specifically, the ratio $R_{21}(N,Z) = Y_2(N,Z)/Y_1(N,Z)$ constructed using the isotope yields $Y_i(N,Z)$ with neutron number N and proton number Z from two different reactions denoted by the index i, $i=1-2$, obeys a simple relationship [22,24,37,38]

$$R_{21}(N,Z) = C\, e^{\alpha N+\beta Z}. \quad (1)$$

Here, C is an overall normalization factor and α and β are isoscaling parameters. This parametrization is discussed in greater detail within the isoscaling section below. If we adopt the convention that reaction 2 is more neutron rich than reaction 1, one expects α to be positive and β to be negative. We have adopted that convention here and have fitted the ratios of the isotopic yields for these four systems to extract the corresponding values for α and β. These values for α and β are given in Table I.

Equation (1), with only three parameters C, α, and β can be used to predict the isotope yields of ^{112}Sn+^{112}Sn as well as the mixed systems, ^{112}Sn+^{124}Sn or ^{124}Sn+^{112}Sn, using the measured yields of one system, ^{124}Sn+^{124}Sn. To illustrate how well this parametrization relates the yields of these four systems, we take the yields of the ^{124}Sn+^{124}Sn system as a reference and use those yields and the fitted values of α and β to predict the yields for the other three systems. The dash and dot-dashed lines in Fig. 2 are the calculated yields for ^{112}Sn+^{112}Sn and ^{112}Sn+^{124}Sn, respectively. For this limited range of asymmetry, these isoscaling parameters can be described by a linear dependence on either the initial N/Z or the asymmetry parameter, $\delta=(N-Z)/(N+Z)$ of the reactions [38]. The excellent agreement between the predicted yields and the data suggests that such scaling law extrapolations may have useful predictive power. For example, we expect

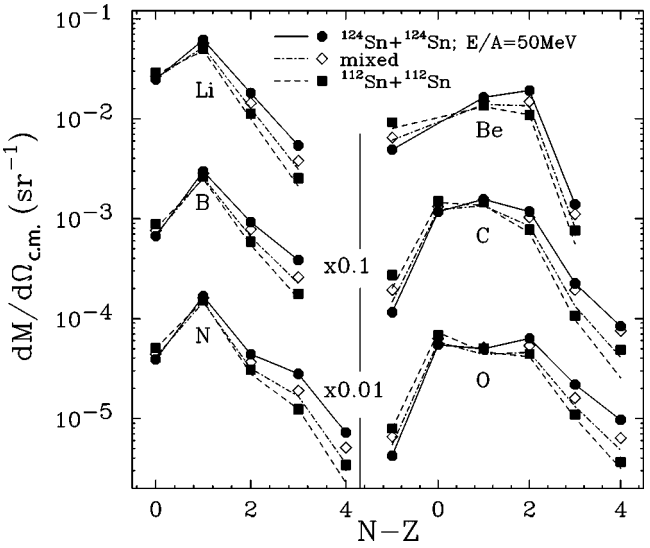

FIG. 2. Average differential multiplicities at $70° \leqslant \theta_{c.m.} \leqslant 110°$ for Li, Be, B, C, N, and O isotopes as a function of neutron excess $(N-Z)$ of the isotope. The solid circles (connected by solid lines to guide the eye) are the data for the ^{124}Sn+^{124}Sn system with $N/Z=1.48$. The solid squares are data for the lightest system ^{112}Sn+^{112}Sn with $N/Z=1.24$. The open diamonds are the averaged values from the two mixed systems, ^{124}Sn+^{112}Sn and ^{112}Sn+^{124}Sn. The dashed and dot-dashed lines are predictions from Eq. (1). See text for more details.

that these scaling predictions can be accurately extrapolated to other mass-symmetric systems of $A=200-250$ nucleons at the same incident energy per nucleon but with very different isospin asymmetry.

III. DESCRIPTION OF THE MODELS

Now we turn to the theoretical interpretation of these data. To study the density dependence of the asymmetry term of the EOS, we adopt the viewpoint of the stochastic mean field (SMF) approach described in Refs. [7,25]. In this approach, the time evolution of the nuclear density is calculated by taking into account both the average phase-space trajectory predicted by the Boltzmann-Nordheim-Vlasov equation and the fluctuations of the individual collision trajectories about this average that can be predicted by equations of the Boltzmann-Langevin type.

The virtue of such a dynamical approach for the study of isotopic effects lies in its self-consistency. The flow of neutrons and protons is calculated under the influence of Coulomb and asymmetry terms, which reflect self-consistently the motion of these nucleons. Several different density dependences of the asymmetry term were explored from which two are selected for presentation here. In both cases, the asymmetry term is approximated by the form

$$E_{sym}(\rho, \delta) = S(\rho)\delta^2, \tag{2}$$

where for the asymmetry term with a stronger density dependence

$$S(\rho) = a\left(\frac{\rho}{\rho_0}\right)^{2/3} + b\frac{2(\rho/\rho_0)^2}{1+(\rho/\rho_0)}. \tag{3}$$

Here, ρ is the physical density, ρ_0 the saturation density, $a=13.4$ MeV and $b=19$ MeV [2,4,39]. In the following, we refer to this as the "superstiff" asymmetry term. For the asymmetry term with weaker density dependence,

$$S(\rho) = a\left(\frac{\rho}{\rho_0}\right)^{2/3} + 240.9\rho - 819.1\rho^2, \tag{4}$$

where $a=12.7$ MeV [27]. In the following, we refer to this as the "soft" asymmetry term. In Fig. 3, it can be seen that the two expressions are nearly equal at saturation density but differ at densities that are either much larger or smaller than ρ_0.

In addition to the asymmetry term, the SMF calculations have a Skyrme-type isoscalar mean field with a soft equation of state for symmetric matter characterized by an incompressibility constant $K=201$ MeV. The isoscalar mean field and the asymmetry term of these equations of state are used for the construction of the initial ground state and for the time evolution of the collision. The nucleon-nucleon collisions by the residual interaction are calculated from an energy and angle dependent parametrization of the free nucleon-nucleon interaction and the isospin dependence of the Pauli blocking is considered during these collisions.

TABLE I. Values for α and β obtained from fitting the isotope ratios R_{21}.

Reaction 2	Reaction 1	α	β
^{112}Sn+^{124}Sn	^{112}Sn+^{112}Sn	0.18±0.01	−0.19±0.01
^{124}Sn+^{124}Sn	^{112}Sn+^{112}Sn	0.36±0.02	−0.39±0.01

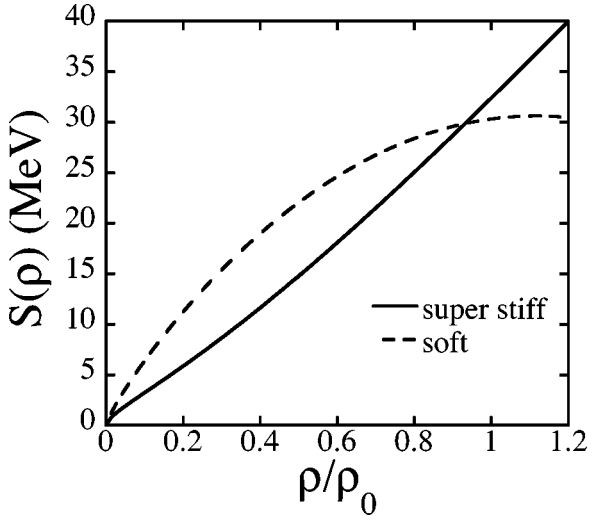

FIG. 3. The solid curve and dashed curves indicate the density dependencies for the super stiff and soft asymmetry terms, respectively.

The calculation solves the transport equations by evolving test particles of finite width. We use a reduced number of test particles (50 test particles per nucleon) in the present calculations to inject numerical noise into the evolution. In test calculations, we alternatively employed the fluctuation mechanism discussed in Ref. [25], which involves damping the numerical noise by utilizing a large number of test particles and introducing explicitly physical noise according to thermal fluctuations. It was checked that both methods lead to similar results. In contrast to the Brownian one-body (BOB) method of Ref. [40], these methods of inserting fluctuations are well suited to reactions at finite impact parameter because they do not presuppose knowledge of the most unstable modes.

When the system expands and reaches the spinodal instability (after about 110–120 fm/c), the most unstable modes are amplified and initiate the formation of fragments via spinodal decomposition. The evolution of the system is continued after spinodal decomposition until freeze-out where the number of dynamically produced fragments and their properties are finally determined. The system is decomposed into fragments using essentially a coalescence mechanism in coordinate space; specifically, fragments are defined by regions of density in the final distributions that are above a "cutoff" density of $1/8\rho_0$. By definition, the freeze-out time occurs when the average calculated number of fragments saturates. This occurs about 260 fm/c after initial contact of projectile and target nuclei in the present simulations. The excitation energy of the fragments is determined by calculating the thermal excitation energy in a local density approximation. The procedure is rather rough and will overestimate the excitation energy particularly for light fragments.

Some of the important features of these calculations and of the prior BUU-SMM [22] and EES [24] calculations can be understood simply by considering the influence of the density dependence of the asymmetry term on the relative emission rates of neutrons and protons. In all Sn+Sn collisions, the symmetry energy in the liquid drop model is positive, i.e., repulsive. The interaction contribution to the symmetry energy gives rise to a repulsive contribution to the mean field potential for neutrons and an attractive contribution to the mean field potential for protons. The mean field potential for an asymmetry term with stronger density dependence is larger at high density and smaller at low density than that for an asymmetry term with weaker density dependence.

It is the low-density behavior that dominates the predictions for the isoscaling parameter. As the system expands and eventually multifragments, the prefragment remains at subnuclear densities for a long time while it is emitting nucleons. The asymmetry term with weaker density dependence around ρ_0 increases the difference between the neutron and proton emission rates leading to a more symmetric prefragment than is produced by calculations with the asymmetry term which has a stronger density dependence.

The SMF calculations are interesting because they are free, in principle, of arbitrary assumptions about whether the fragments are formed at the surfaces or from the bulk disintegration of the system. Comparisons between the fragmentation dynamics for different asymmetry terms were reported in Ref. [41]. The trends of these calculations are consistent with the prefragment isospin dependences discussed above. In particular, fragments produced in calculations with an asymmetry term with strong density dependence tend to be more neutron rich than the fragments produced in calculations with an asymmetry term with weak density dependence. In this respect, these predictions are similar to the results of the BUU-SMM calculations of Ref. [22] and opposite to the results of the EES calculations of Ref. [24].

However, the SMF fully dynamical formation of fragments should actually be more sensitive than the hybrid BUU-SMM to the interplay of the EOS, i.e., to the density dependence of the asymmetry term, with the fragmentation process. In the hybrid BUU-SMM calculations, the EOS is entering only in the "preequilibrium" nucleon emission described above. In the SMF approach, we have not only this isospin effect on fast particle emission but also the full dynamics of the isospin fractionation/distillation mechanism during the cluster formation. In a neutron-rich system, this leads to a different N/Z "concentration" in the liquid phase (the fragments are more symmetric) and in the gas phase (nucleons and light ions, are more neutron rich) [18,42]. This effect is associated with the unstable behavior of dilute asymmetric nuclear matter and so in this way we have the chance of testing the EOS also at subsaturation density.

Asymmetry terms with weaker density dependence around ρ_0 must show a faster increase at low densities and so a larger isospin fractionation/distillation during the fragment formation [7]. Therefore in a fully dynamical picture of fragmentation events a soft behavior of the asymmetry term around saturation density will enhance the formation of more symmetric fragments for two converging reasons: (i) A larger preequilibrium neutron emission rate as discussed before; (ii) a stronger isospin fractionation/distillation during the bulk disintegration. Opposite effects are of course predicted for a rapidly increasing ("stiff") asymmetry term around ρ_0. In this sense we can expect the SMF results to be more sensitive to the isospin dependences of the EOS at subsaturation density.

At freeze-out, the fragments are highly excited. For simplicity, we assume that the deexcitation of these fragments can be calculated as if the fragments are isolated. For this deexcitation stage, we have tabulated the known masses, states, spins, isospins, and branching ratios for nuclei with $Z \leqslant 15$. Where experimental information is complete, it is used. Alternatively, empirical level density expressions are used for the discrete levels. These discrete levels are matched to continuum level density expressions as described in Ref. [31]. The decay of primary fragments with $Z \geqslant 15$ are calculated, following Ref. [31], using known branching ratios, when available, and using the Hauser-Feshbach formalism when the information is lacking. The decays of heavier nuclei are calculated using the Gemini statistical decay code [31,43].

While the SMF calculations predict the numbers and properties of the hot fragments that are produced at breakup, the predictions for the relative abundances of light clusters such as the isotopes with $Z=1-2$ that are emitted before the system expands to subnuclear density are not very realistic. This prevents a precise modeling of complete events including their detection efficiency and means that the impact pa-

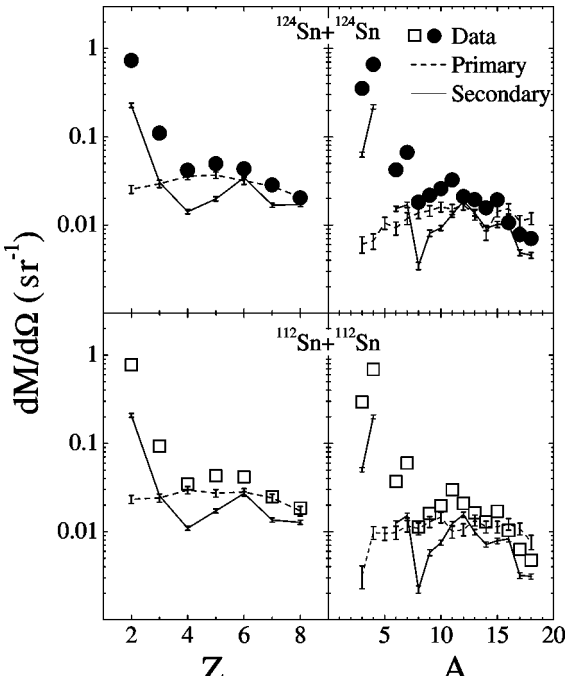

FIG. 4. Differential multiplicities for ^{112}Sn+^{124}Sn collisions (upper panel) and ^{112}Sn+^{112}Sn collisions (lower panel) as a function of the fragment charge (left panels) and the fragment mass (right panels). The points are the data. The dashed and solid lines are the calculated primary and final fragment differential multiplicities, respectively. Statistical uncertainties are shown for the calculations; the corresponding uncertainties in the data are smaller than the data points.

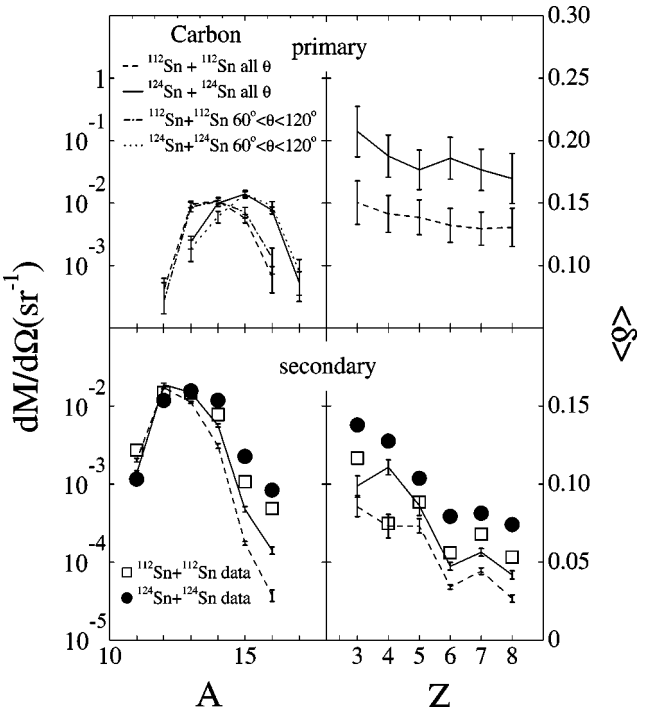

FIG. 5. Left panels: Calculated primary (upper panel), calculated final (lower panel), and measured (lower panel) carbon isotopic yields for Sn+Sn collisions. Right panels: Calculated primary (upper panel), calculated final (lower panel), and measured (lower panel) mean isospin asymmetries as a function of the fragment charge for Sn+Sn collisions. The lines and data points are further explained in the text.

rameter selection based on multiplicity cannot be imposed straightforwardly on the calculated events as on the data. This and the considerable numerical effort it requires have persuaded us to limit our comparisons to calculations composed of 600 events for each of the ^{112}Sn+^{112}Sn and ^{124}Sn +^{124}Sn reactions at a fixed impact parameter of $b=2$ fm. We note, however, that the widths in the multiplicity distributions at fixed impact parameter are large enough that a range of impact parameters may contribute significantly to the experimental data. Future calculations are necessary to assess quantitatively the importance of this impact parameter smearing.

IV. OVERALL BEHAVIOR PREDICTED BY THE SMF CALCULATIONS

In Fig. 4, the solid circles and open squares in the left panel show the measured elemental multiplicities for $2 \leqslant Z \leqslant 8$ averaged over $70° \leqslant \theta_{\mathrm{c.m.}} \leqslant 110°$ for ^{124}Sn+^{124}Sn and ^{112}Sn+^{112}Sn collisions, respectively. The right panels show the corresponding measured multiplicities as a function of the fragment mass. These averaged multiplicities were obtained by summing the isotopic multiplicities for $2 \leqslant Z \leqslant 8$.

The dashed lines denote the corresponding distributions of hot primary fragments calculated by the SMF model using the superstiff EOS. Due to the low total number of events, we averaged these calculations over a slightly larger angular interval of $60° \leqslant \theta_{\mathrm{c.m.}} \leqslant 120°$. The solid lines show the multiplicities of cold fragments after secondary decay. The statistical uncertainties in these calculations are shown in the figure as vertical bars. The corresponding uncertainties in the data are smaller than the data points. If the angular integration was performed over the entire solid angle, the averaged calculated multiplicities are about 20–30 % larger. This difference reflects an anisotropy in the calculated primary angular distributions for the heavier fragments. In the present calculations, however, we do not have the capability to accurately calculate the modifications of the angular distribution due to secondary decay so we presently cannot explore this issue more quantitatively. As we will show later, this anisotropy has no impact on the shapes of the isotopic distributions for $Z=3-8$.

In general, the calculated primary and secondary fragment multiplicities are smaller than the measured values for the lighter fragments $Z=3,4$ and are somewhat closer to the measured values for $Z=6-8$. The lighter fragments with $Z<4$ are mainly produced in secondary decay stage of the theoretical calculations; the primary yields of these light fragments are much smaller relative to the final yields than are the values for the heavier fragments. Because the fragment multiplicities and angular distributions depend on impact parameter, the comparison shown in Fig. 4 may be sensitive to the impact parameter ranges included in both calculation and data. Future calculations over a wide range of impact parameters are needed to address this issue. Con-

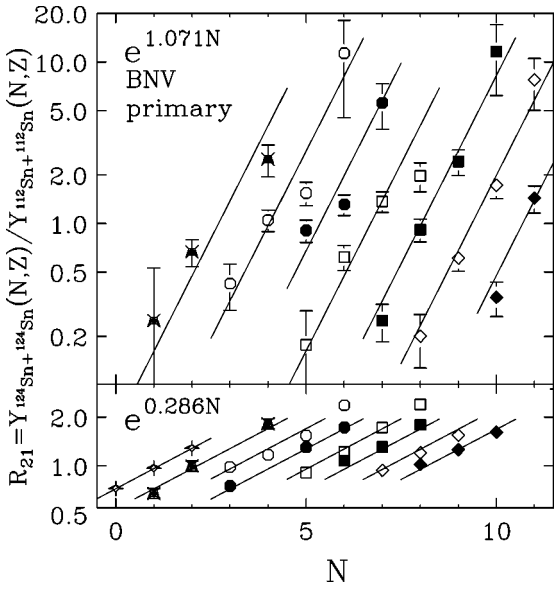

FIG. 6. Upper panel: R_{21} values obtained from the ratios of the primary isotopic distributions for ^{124}Sn+^{124}Sn collisions divided by those for ^{112}Sn+^{112}Sn collisions. Lower panel: Corresponding R_{21} values obtained from the ratios of the final isotopic distributions. Each line in the two panels corresponds to ratios for a given element. Elements with $Z=2-8$ ($Z=1-8$) are represented from left to right in the upper (lower) panel. The lines are the result of fitting R_{21} with Eq. (1); the dependencies on neutron number for the best fits are given in each panel.

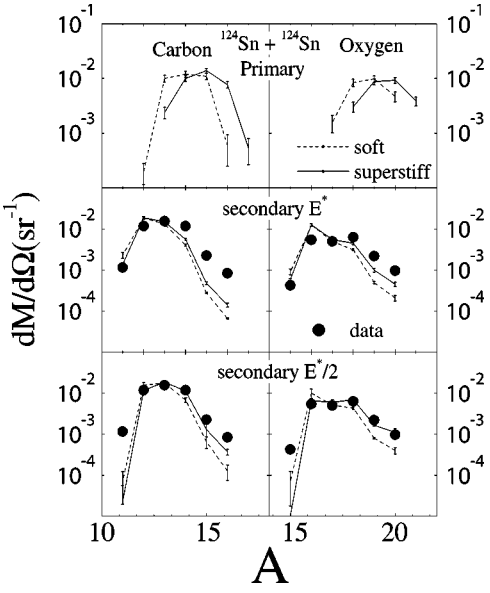

FIG. 7. Upper panel: Dependence of the primary distributions for carbon (left panel) and oxygen (right panel) upon the density dependence of the asymmetry term. Middle panel: Dependence of the final distributions for carbon (left panel) and oxygen (right panel) upon the density dependence of the asymmetry term. The data are also shown as the solid points. The various lines in the figure are described in the text. The excitation energies for the fragments are taken directly from the SMF calculations. Lower panel: The data are the same as in the middle panels. The curves are the calculations obtained when the excitation energies of the primary fragments are reduced by a factor of 2.

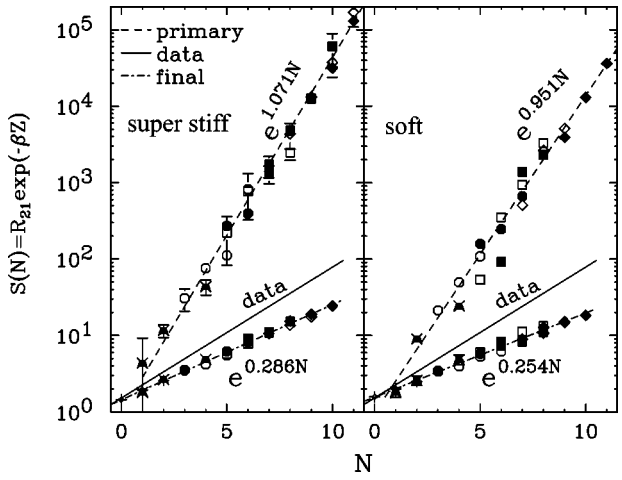

FIG. 8. Dependence of the scaled function $S(N)$ on the density dependence of the asymmetry term. The left panel provides a comparison between values for $S(N)$ computed from the data (solid line) and the calculated primary (points about the dashed line) and final (points about the dotted-dashed line) distributions obtained for the superstiff asymmetry term. The right panel provides a comparison between values for $S(N)$ computed from the data and the calculated primary and final distributions obtained for the soft asymmetry term.

cerning the greater discrepancy for $Z=2-4$ fragments, we have already noted that the formation of light clusters in the dynamical stage before breakup is not well described in BUU- and SMF-type simulations, because the unique structural properties of these fragments are not well treated therein. (Treatments of the emission of light clusters in coupled transport equations for nucleons and light clusters can be found in Refs. [44,45] and in the framework of FMD [46] or AMD [47] simulations.) On the other hand, there is a considerable emission of protons and neutrons during this stage; the total emission and consequently the asymmetry of the remaining source may still be realistic.

Now we turn to an examination of calculated isotopic yields. The upper left panel of Fig. 5 shows the isotopes of carbon nuclei predicted by the SMF calculations over the entire angular range for ^{124}Sn+^{124}Sn (solid line) and ^{112}Sn +^{112}Sn (dashed line); the dotted-dashed and dotted lines show the corresponding calculations over the $60° \leqslant \theta_{\mathrm{c.m.}} \leqslant 120°$ gate. Not surprisingly, the more neutron-rich ^{124}Sn +^{124}Sn system preferentially produces the more neutron-rich isotopes. The peak of the carbon primary distribution for the ^{124}Sn+^{124}Sn system occurs at about ^{15}C while the peak for ^{112}Sn+^{112}Sn system occurs at lower mass, i.e., somewhere between ^{13}C and ^{14}C. The differences between the angle gated and total primary yields are small, and these differences translate into negligible differences in the shape of the isotopic yield distribution after secondary decay; we therefore do not plot the gated data because the two curves are indistinguishable when normalized to each other. As the statistics of the present calculation make it difficult to perform comparisons to isotopic yields with a $60° \leqslant \theta_{\mathrm{c.m.}} \leqslant 120°$ gate imposed on the calculation, the remaining calculated multiplicities in the paper are integrated over the entire solid angle.

After sequential decays, one obtains the secondary distributions shown in the lower left panel. There is no longer a noticeable difference between the peak locations (at ^{12}C in both systems); instead, the main differences are found in the shape of the distribution, which is higher in the neutron-rich isotopes and lower in the neutron-deficient isotopes for the ^{124}Sn+^{124}Sn system than it is for the ^{112}Sn+^{112}Sn system. Such trends are also qualitatively observed in the experimental data shown for the ^{124}Sn+^{124}Sn system by the solid circles and for the ^{112}Sn+^{112}Sn system by the open squares in the lower left panel. However, the experimental distributions are considerably wider and more neutron rich than the model predictions. This trend is replicated in the isotopic distributions for all of the other measured elements.

Another way to quantify the differences in the isotope distributions is by the asymmetry parameter $\delta=(N-Z)/(N+Z)$. The average asymmetry $\langle\delta\rangle$ of the isotopic distribution for each element is shown as a function of Z in the right panels of Fig. 5. Following the same convention as in the left panels, the solid and dashed lines show the average asymmetries for ^{124}Sn+^{124}Sn and ^{112}Sn+^{112}Sn collisions; the upper and lower panels present results for the primary and secondary fragment distributions, respectively. The calculated differences between the two systems are more pronounced prior to secondary decay than afterwards. The asymmetries of the corresponding data, shown for the ^{124}Sn+^{124}Sn system by the solid circles and for the ^{112}Sn+^{112}Sn system by the open squares in the lower right panel, are larger and display a stronger dependence on the asymmetry of the system than do the final calculated fragment yields after secondary decay.

V. ISOSCALING ANALYSES

A more sensitive way to compare isotopic distributions is to construct the isotopic ratio $R_{21}(N,Z)=Y(N,Z)=Y_2(N,Z)/Y_1(N,Z)$ from the isotope yields $Y_i(N,Z)$ with neutron number N and proton number Z from two different reactions. As discussed in the experimental section, $R_{21}(N,Z)$ obeys a simple relationship $R_{21}(N,Z)=Ce^{\alpha N+\beta Z}$, where C is an overall normalization factor and α and β are isoscaling parameters [22,24,37,38]. Such an isoscaling relationship can be obtained in statistical theories for two systems that are at the same temperature when they produce fragments. Binding energy factors common to the yields for the fragments in each system are canceled by the ratio when the temperatures are equal, leaving terms related to the chemical potentials or separation energies [24]. In grand canonical models of multifragmentation $\alpha=\Delta\mu_p/T$ and $\beta=\Delta\mu_n/T$, for example, $\Delta\mu_n$, $\Delta\mu_p$ are the differences in the chemical potentials for the neutrons and protons in the two systems and T is the temperature [37,38]. In some calculations [38], the values for the isoscaling parameters extracted from equilibrium multifragmentation models are similar before and after sequential decays, an observation that has been attributed to a partial cancellation of secondary decay effects [37,38].

While isoscaling can be expected for many statistical processes [22,24,37,38], the question of whether it can be expected for specific dynamical calculations remains open. To investigate whether the SMF dynamical model displays isoscaling, we construct the relative isotope ratios R_{21} primary, using the primary fragments produced in ^{124}Sn+^{124}Sn collisions as reaction 2 (numerator) and in ^{112}Sn+^{112}Sn collisions as reaction 1 (denominator).

The results are shown in the upper panel of Fig. 6. The error bars reflect the statistical uncertainties. The predicted isotope ratios for these primary fragments depend very strongly on the neutron number and follow trends that appear consistent with isoscaling relationship defined by Eq. (1). The uncertainties are large reflecting the low statistics of the simulations, but the strong dependence on neutron number makes it possible to discern apparent isoscaling trends nonetheless. The lines are best fits using Eq. (1) resulting in $C=0.96$, $\alpha=1.07$, and $\beta=-1.43$. These values for α are much larger than values observed in the experiment. The lower panel provides the corresponding SMF predictions for the ratios $R_{21,final}$ of the yields of particle stable nuclei after secondary decay. For comparison purposes, the scale for the ordinates of the top and bottom panels are chosen to be the same; this demonstrates graphically that the trends of the final isotope ratios are much flatter and the corresponding isoscaling parameters ($\alpha=0.286$ and $\beta=-0.288$) are much smaller. Clearly, the isoscaling parameters predicted by dynamic SMF calculations are strongly modified by secondary decay. This trend is very different from some equilibrium statistical models for multifragmentation where the isoscaling parameters have been predicted to be insensitive to secondary decay [37,38].

The isoscaling behavior of the dynamically produced fragments arises not from thermal physics but rather from some special characteristics of the SMF primary distributions predicted for these reactions. We find, for example, the SMF primary isotopic and isotonic distributions can be roughly described by Gaussians, see Fig. 4 [48]. Isotopic distributions, for example, can be described by

$$Y(N,Z)=f(Z)\exp\left[-\frac{[N-\overline{N}(Z)]^2}{2\sigma_Z^2}\right], \tag{5}$$

where $\overline{N}(Z)$ is the centroid of the distribution and σ_Z^2 describes the width of the distribution for each element of charge Z. This leads to an exponential behavior of the ratio R_{21}, since, neglecting quadratic terms in $\overline{N}$,

$$\ln R_{21}=\frac{1}{\sigma_Z^2}[\overline{N}(Z)_2-\overline{N}(Z)_1]N. \tag{6}$$

Note Eq. (6) requires the values for σ_Z^2 to be approximately the same for both reactions. We have observed this to be the case for our SMF calculations of Sn+Sn collisions (to within the statistical accuracy $\sim$10%). For the ratios for every element, to be optimally described by the same parameter, the ratio must be independent of Z. The statistics of the calculation do not allow a detailed test of this assumption, but it does appear that $[\overline{N}(Z)_2-\overline{N}(Z)_1]/\sigma_Z$ increases somewhat with Z, as Fig. 6 suggests. The primary

distributions therefore do not respect the isoscaling relationship as well the data do.

Now, at variance with the statistical fragmentation models, the secondary decays substantially modify the isoscaling parameter. The width σ_Z^2 decreases due to secondary decay and the difference $[N_2-N_1]$ likewise decreases fractionally, but by a larger amount. Moreover, the final shape is no longer Gaussian, but due to secondary decay, it reflects the binding energy as a function of neutron excess more strongly (see Fig. 5). These changes combine to decrease the isoscaling parameter as shown in the lower panel of Fig. 6.

VI. SENSITIVITY OF THE SMF CALCULATIONS TO THE ASYMMETRY TERM

The density dependence of the asymmetry term has a significant influence on the relative emission rates of the neutrons and protons and, consequently, on the isospin asymmetry of the hot fragments prior to secondary decay. As discussed previously, an asymmetry term with weaker density dependence tends to remain more important at lower densities, driving the fragments closer to isospin symmetry, than does an asymmetry term with stronger density dependence. Consistent with this general consideration, the calculated primary isotope distributions in $^{124}Sn+^{124}Sn$ collisions, shown in Fig. 7 for carbon (upper left panel) and oxygen (upper right panel), are more neutron rich for the superstiff asymmetry term (solid line) than they are for the soft asymmetry term (dashed line). A similar trend is also predicted for the $^{112}Sn+^{112}Sn$ system, but is not shown in the interest of brevity.

A similar trend is observed in the corresponding final distributions that are obtained after secondary decay and shown in the middle panel with the same convention for the solid and dashed lines as in the upper panel. Both secondary distributions calculated for superstiff and soft asymmetry terms, however, are significantly narrower and more proton rich than the experimental distributions shown by the closed circles in the figure. (The lower panels, which display corresponding calculations when the excitation energy is reduced by 50%, will be discussed in the following section of this paper.) Similar trends are also observed for the $^{112}Sn+^{112}Sn$ and for the other elements with $3 \leqslant Z \leqslant 8$, though we do not for brevity's sake show those results.

In Fig. 8, we present the related dependence of the SMF predictions for the isotope ratios R_{21} upon the density dependence of the asymmetry term. We take advantage of the fact that the results in Fig. 6 can be compactly displayed by the scaled function $S(N)=R_{21}(N,Z)e^{-\beta Z}$, which condenses the isotopic dependence for the various elements onto a single line [24]. The left panel in Fig. 8 shows the results for the superstiff asymmetry term and the right panel shows the results for the soft asymmetry term. In each panel, the values for $S(N)$ obtained from the primary distribution are shown by the symbols clustered about the dashed lines, the results obtained from the secondary distribution are shown by the symbols clustered about the dotted-dashed lines, and the results from the data are shown by the solid lines in each panel to provide a reference. Both the primary and secondary values for $S(N)$ have been fit by exponential functions to obtain corresponding values for the scaling parameter and these values are given in the figure.

Generally, the primary distributions for both equations of state display a much stronger dependence on neutron number than do the final isotopic distributions and the data. However, the influence on the isoscaling parameter is statistically not very significant. Indeed, as we pass from a stiff asymmetry term to a soft one, we do have a stronger isospin fractionation/distillation, as already discussed before. The centroid of the distribution N_2 decreases (see Fig. 7) but also the width σ_Z^2 decreases; the decrease in width, however, is of the order of 10% and comparable to its statistical uncertainty. The calculated final distributions display a weak sensitivity to the density dependence of the asymmetry term; the values for ($\alpha=0.286$) obtained for the superstiff asymmetry term are larger than the values for ($\alpha=0.254$) obtained for the soft asymmetry term. The sensitivity to the asymmetry term is considerably less than that reported for the EES model [24] and for the BUU-SMM hybrid calculations [22]. Unlike these latter two calculations, both superstiff and soft asymmetry terms yield α values that are significantly lower than the value extrapolated from the data ($\alpha=0.36$). One should note, however, that the excitation energies of these latter calculations could be more freely varied to achieve better agreement with the experimental observations.

VII. DISCUSSION AND SUMMARY

The calculated final isotopic distributions for both asymmetry terms differ from the measured ones in that they are narrower; more neutron deficient; and show a weaker dependence on the isotopic asymmetry of the total system. The last characteristic is reflected more clearly by the isoscaling parameter than by direct examination of the isotopic distributions, themselves. In these respects, the calculated results for the two different asymmetry terms are more similar to each other than they are to the data. We believe that it is probably premature at this stage to focus attention on the sensitivity of the predicted final distributions to the asymmetry term. Instead, let us concentrate upon what may be required to bring the final isotopic distributions into greater concordance with the measurements.

The tendencies of the final isotopic distributions to be more neutron deficient and to display a weaker dependence on the isotopic asymmetry of the system are somewhat related. Both point to difficulties the present calculations have in producing neutron-rich isotopic distributions and indicate a surprising sensitivity of the final results to the primary distributions. That the final isotopic distributions are too neutron deficient may result from the primary distributions being too neutron deficient on the average, too narrow (i.e., σ_Z is too small) or that the secondary decay calculations predict too much neutron emission after freeze-out because the calculated excitation energies are too high or the excitation energy distributions are too narrow resulting in the loss of com-

ponents at low excitation energies that could decay to neutron-rich final products.

We note that additional experimental measurements may help to resolve these questions. The average isospin asymmetry of the initial distributions is trivially related by charge and mass conservation to the average isospin asymmetry of the nucleons emitted during the SMF calculations before the freeze-out ($t=260$ fm/c) chosen for these calculations. Complimentary measurements of the yields and energy spectra of light particles can help to determine whether these missing neutrons are carried away primarily by pre-equilibrium emission during the compression-expansion stage or during the later evaporative decay of the hot fragments.

Previous authors have identified issues relevant to our calculations, which may influence the asymmetries of the hot fragments at freeze-out [45,49,50]. As discussed above, the present simulations underestimate the emission of light clusters (d, t, ^{3}He, ^{4}He, ^{6}Li, ^{7}Li, etc.) during the dynamical evolution prior to the freeze-out. Previous studies [45,49,50] have noted that the neglect of the emission of ^{4}He emission is particularly problematic because it is abundant and because each ^{4}He particle enhances the isospin asymmetry of the remaining system by removing four nucleons without changing the neutron excess. Indeed, it has been speculated that ^{4}He emission may have an influence on the isospin asymmetry of the other clusters and fragments that is of the same order of magnitude as the influence of the mean field [45,49,50]. The issue needs additional theoretical attention.

Concerning neutron emission after freeze-out, we note that the number of neutrons removed by secondary decay depends primarily on the fragment excitation energies and the relative branching ratios for neutron and charged-particle emission. There are significant uncertainties in the calculation of the excitation energies of the fragments, which are related to the difficulty to establishing their precise ground state binding energies. To explore the sensitivity of the results to the excitation energy, we have reduced the excitation energy of each fragment by a multiplicative factor f, where $0.5 \leqslant f \leqslant 1$ and recalculated the final fragment isotopic distributions.

The solid and dashed lines in Fig. 7 for carbon fragments (lower left panel) and oxygen fragments (lower right panel) show the calculated final distributions for $f=0.5$ using superstiff and soft asymmetry terms, respectively. Clearly, it is possible by reducing the excitation energy to shift the isotope distribution in the direction of the more neutron-rich isotopes, so as to make the mean isospin asymmetry of the calculated final and measured distributions to be the same. However, the widths of the calculated final isotopic distributions will still be narrower than the measured ones.

This discrepancy between the theoretical and experimental widths would be reduced if the theoretical primary distributions were wider in their excitation energy distributions or wider in their isotopic distributions or both. The primary distributions of equilibrium statistical model calculations that reproduce the experimental final distributions are much wider in excitation energy and neutron number than those predicted by the SMF calculations [23,31,38]. Future investigations will be needed to address whether wider primary distributions in excitation energy or neutron number can be attained in the SMF model by altering some of the underlying model assumptions such as the manner in which they are defined at freeze-out.

Increased widths may be achieved by performing calculations for a range of impact parameters rather than the single impact parameter $b=2$ fm presented here. For example, the inclusion of larger impact parameter events could broaden the primary distributions at midrapidity because it will require the inclusion of fragments emitted from the neck joining projectile- and target-like residues. Also, SMF calculations predict such "neck" fragments to be more neutron rich because the isospin fractionation/distillation effect is somewhat reduced in peripheral events, leaving more neutrons in the fragments, and there can also be an overall neutron enhancement in the neck region for such events due to the neutron skins of the projectile and target [7]. In addition, the excitation energies of the primary fragments in more peripheral collisions are also somewhat reduced. Experiments also suggest that neck fragments in very-peripheral collisions are more neutron rich [51]. But these same measurements show the observation neutron-rich neck fragments to be associated with events in which projectile-like remnants survive the collision. One also expects to observe prominent Coulomb-holes in the fragment and charged-particle emission patterns due to the Coulomb repulsion by these heavy remnants. Neither projectile remnants nor Coulomb holes are observed for the central collisions analyzed here (see Fig. 1), even though both are obvious at larger impact parameter selections of about $b/b_{\max} \approx 0.8$ [52]. Thus, the likelihood of an explanation of these discrepancies in terms of significant contributions of neck fragments from more peripheral collisions appears remote.

In summary, we have measured the isotope distributions of $Z=2-8$ particles emitted in four different Sn+Sn reactions with different isospin asymmetry and have calculated them with a dynamical model that includes fluctuations that give rise to fragment production. The experimental data display a strong dependence on the isospin asymmetry that can be accurately described by an isoscaling parametrization. The theoretical calculations reproduce the yields for the heavier fragments with $Z=6-8$, but underpredict the yields of the lighter ones, which are not strongly produced as primary fragments. The calculated final isotopic distributions display isoscaling, but the calculated isotopic distributions are narrower, more neutron deficient; and show a weaker dependence on the isotopic asymmetry of the system than do the data. The density dependence of the asymmetry term of the EOS has an effect on the calculated final isotopic distributions. The distributions calculated using the asymmetry term with stronger density dependence are more neutron rich and are closer to the measured values. These trends are similar to prior results obtained for a BUU-SMM hybrid model, but different from the trends for evaporated fragments predicted by EES rate equation calculations. The present level of agreement between theory and experiment precludes definitive statements about the density dependence of the asymmetry term of the EOS, but it does reveal that final distributions are surprisingly sensitive to the widths predicted by the SMF model for the primary fragment isotope and excitation energy distributions. A number of theoretical

issues, such as the preequilibrium emission of bound clusters, the calculations of fragment excitation energies, the way fragments are defined at freeze-out, and the impact parameter range modeled by the calculation may influence the calculated results. Additional theoretical work is required to explore these issues and to determine the role they may play in the resolution of these discrepancies. Complementary measurements of the isospin asymmetry of light cluster emission prior to the multifragment breakup can provide information relevant to the resolution of these issues.

ACKNOWLEDGMENTS

This work was supported by the National Science Foundation under Grants Nos. PHY-95-28844 and PHY-0070818, by the U.S. Department of Energy under Contract Nos. DE-FG02-92ER-40714 and DE-FG02-87ER-40316, and by the INFN of Italy. Some of the authors benefited from the scientific environment of a workshop at the European Centre for Theoretical Studies in Nuclear Physics, Trento where this work was extensively discussed.

[1] *Isospin Physics in Heavy-Ion Collisions at Intermediate Energies*, edited by Bao-An Li and W. Udo Schroeder (NOVA Science, New York, 2001).
[2] J. M. Lattimer and M. Prakash, Astrophys. J. **550**, 426 (2001) and references therein.
[3] B. Alex Brown, Phys. Rev. Lett. **85**, 5296 (2000).
[4] Bao-An Li, Phys. Rev. Lett. **85**, 4221 (2000).
[5] L. Scalone, M. Colonna, and M. Di Toro, Phys. Lett. B **461**, 9 (1999).
[6] V. Baran, M. Colonna, M. Di Toro, and A. B. Larionov, Nucl. Phys. **A632**, 287 (1998).
[7] V. Baran, M. Colonna, M. Di Toro, V. Greco, M. Zielinska-Pfabé, and H. H. Wolter, Nucl. Phys. **A703**, 603 (2002).
[8] N. Marie, R. Laforest, R. Bougault, J. P. Wieleczko, D. Durand, Ch. O. Bacri, J. F. Lecolley, F. Saint-Laurent, G Auger, J. Benlliure, E. Bisquer, B. Borderie, R. Brou, J. L. Charvet, A. Chbihi, J. Colin, D. Cussol, R. Dayras, E. De Filippo, A. Demeyer, D. Doré, P. Ecomard, P. Eudes, D. Gourio, D. Guinet, P. Lautesse, J. L. Laville, A. Le Fèvre, T. Lefort, R. Legrain, O. Lopez, M. Louvel, V. Métivier, L. Nalpas, A. Ouatizerga, M. Parlog, J. Péter, E. Plagnol, A. Rahmani, T. Reposeur, M. F. Rivet, E. Rosato, S. Salou, M. Squalli, J. C. Steckmeyer, B. Tamain, L. Tassan-Got, E. Vient, and C. Volant, Phys. Lett. B **391**, 15 (1997).
[9] C. Williams, W. G. Lynch, C. Schwarz, M. B. Tsang, W. C. Hsi, M. J. Huang, D. R. Bowman, J. Dinius, C. K. Gelbke, D. O. Handzy, G. J. Kunde, M. A. Lisa, G. F. Peaslee, L. Phair, A. Botvina, M-C. Lemaire, S. R. Souza, G. Van Buren, R. J. Charity, L. G. Sobotka, U. Lynen, J. Pochodzalla, H. Sann, W. Trautmann, D. Fox, R. T. de Souza, and N. Carlin, Phys. Rev. C **55**, R2132 (1997).
[10] M. D'Agostino, A. S. Botvina, P. M. Milazzo, M. Bruno, G. J. Kunde, D. R. Bowman, L. Celano, N. Colonna, J. D. Dinius, A. Ferrero, M. L. Fiandri, C. K. Gelbke, T. Glasmacher, F. Gramegna, D. O. Handzy, D. Horn, W. C. Hsi, M. Huang, I. Iori, M. A. Lisa, W. G. Lynch, L. Manduci, G. V. Margagliotti, P. F. Mastinu, I. N. Mishustin, C. P. Montoya, A. Moroni, G. F. Peaslee, F. Petruzzelli, L. Phair, R. Rui, C. Schwarz, M. B. Tsang, G. Vannini, and C. Williams, Phys. Lett. B **371**, 175 (1996).
[11] D. R. Bowman, G. F. Peaslee, N. Carlin, R. T. de Souza, C. K. Gelbke, W. G. Gong, Y. D. Kim, M. A. Lisa, W. G. Lynch, L. Phair, M. B. Tsang, C. Williams, N. Colonna, K. Hanold, M. A. McMahan, G. J. Wozniak, and L. G. Moretto, Phys. Rev. Lett. **70**, 3534 (1993).
[12] E. Cornell, T. M. Hamilton, D. Fox, Y. Lou, R. T. de Souza, M. J. Huang, W. C. Hsi, C. Schwarz, C. Williams, D. R. Bowman, J. Dinius, C. K. Gelbke, T. Glasmacher, D. O. Handzy, M. A. Lisa, W. G. Lynch, G. F. Peaslee, L. Phair, M. B. Tsang, G. VanBuren, R. J. Charity, L. G. Sobotka, and W. A. Friedman, Phys. Rev. Lett. **75**, 1475 (1995).
[13] R. Popescu, T. Glasmacher, J. D. Dinius, S. J. Gaff, C. K. Gelbke, D. O. Handzy, M. J. Huang, G. J. Kunde, W. G. Lynch, L. Martin, C. P. Montoya, M. B. Tsang, N. Colonna, L. Celano, G. Tagliente, G. V. Margagliotti, P. M. Milazzo, R. Rui, G. Vannini, M. Bruno, M. D'Agostino, M. L. Fiandri, F. Gramegna, A. Ferrero, I. Iori, A. Moroni, F. Petruzzelli, P. F. Mastinu, L. Phair, and K. Tso, Phys. Rev. C **58**, 270 (1998).
[14] G. J. Kunde, S. J. Gaff, C. K. Gelbke, T. Glasmacher, M. J. Huang, R. Lemmon, W. G. Lynch, L. Manduci, L. Martin, M. B. Tsang, W. A. Friedman, J. Dempsey, R. J. Charity, L. G. Sobotka, D. K. Agnihotri, B. Djerroud, W. U. Schröder, W. Skulski, J. Tõke, and K. Wyrozebski, Phys. Rev. Lett. **77**, 2897 (1996).
[15] N. Marie, A. Chbihi, J. B. Natowitz, A. Le Fèvre, S. Salou, J. P. Wieleczko, L. Gingras, M. Assenard, G. Auger, Ch. O. Bacri, F. Bocage, B. Borderie, R. Bougault, R. Brou, P. Buchet, J. L. Charvet, J. Cibor, J. Colin, D. Cussol, R. Dayras, A. Demeyer, D. Doré, D. Durand, P. Eudes, J. D. Frankland, E. Galichet, E. Genouin-Duhamel, E. Gerlic, M. Germain, D. Gourio, D. Guinet, K. Hagel, P. Lautesse, J. L. Laville, J. F. Lecolley, T. Lefort, R. Legrain, N. Le Neindre, O. Lopez, M. Louvel, Z. Majka, A. M. Maskay, L. Nalpas, A. D. Nguyen, M. Parlog, J. Péter, E. Plagnol, A. Rahmani, T. Reposeur, M. F. Rivet, E. Rosato, F. Saint-Laurent, J. C. Steckmeyer, M. Stern, G. Tabacaru, B. Tamain, O. Tirel, E. Vient, C. Volant, and R. Wada, Phys. Rev. C **58**, 256 (1998).
[16] W. A. Friedman, Phys. Rev. C **42**, 667 (1990).
[17] J. P. Bondorf, A. S. Botvina, A. S. Iljinov, L. N. Mishustin, and K. Sneppen, Phys. Rep. **257**, 133 (1995), and references therein.
[18] H. Müller and B. D. Serot, Phys. Rev. C **52**, 2072 (1995).
[19] D. H. E. Gross, Phys. Rep. **279**, 119 (1997).
[20] B. Borderie, G. Tăbăcaru, Ph. Chomaz, M. Colonna, A. Guarnera, M. Pârlog, M. F. Rivet, G. Auger, Ch. O. Bacri, N. Bellaize, R. Bougault, B. Bouriquet, R. Brou, P. Buchet, A. Chbihi, J. Colin, A. Demeyer, E. Galichet, E. Gerlic, D. Guinet, S. Hudan, P. Lautesse, F. Lavaud, J. L. Laville, J. F. Lecolley, C. Leduc, R. Legrain, N. Le Neindre, O. Lopez, M. Louvel, A. M. Maskay, J. Normand, P. Pawłowski, E. Ro-

sato, F. Saint-Laurent, J. C. Steckmeyer, B. Tamain, L. Tassan-Got, E. Vient, and J. P. Wieleczko, Phys. Rev. Lett. **86**, 3252 (2001).

[21] R. Wada, K. Hagel, J. Cibor, M. Gonin, Th. Keutgen, M. Murray, J. B. Natowitz, A. Ono, J. C. Steckmeyer, A. Kerambrum, J. C. Angélique, A. Auger, G. Bizard, R. Brou, C. Cabot, E. Crema, D. Cussol, D. Durand, Y. El Masri, P. Eudes, Z. Y. He, S. C. Jeong, C. Lebrun, J. P. Patry, A. Péghaire, J. Peter, R. Régimbart, E. Rosato, F. Saint-Laurent, B. Tamain, and E. Vient, Phys. Rev. C **62**, 034601 (2000).

[22] W. P. Tan, B.-A. Li, R. Donangelo, C. K. Gelbke, M.-J. van Goethem, X. D. Liu, W. G. Lynch, S. Souza, M. B. Tsang, G. Verde, A. Wagner, and H. S. Xu, Phys. Rev. C **64**, 051901(R) (2001).

[23] S. R. Souza, W. P. Tan, R. Donangelo, C. K. Gelbke, W. G. Lynch, and M. B. Tsang, Phys. Rev. C **62**, 064607 (2000).

[24] M. B. Tsang, W. A. Friedman, C. K. Gelbke, W. G. Lynch, G. Verde, and H. S. Xu, Phys. Rev. Lett. **86**, 5023 (2001).

[25] M. Colonna, M. Di Toro, A. Guarnera, S. Maccarone, M. Zielinska-Pfabé, and H. H. Wolter, Nucl. Phys. **A642**, 449 (1998).

[26] M. Di Toro, V. Baran, M. Colonna, and V. Greco, Prog. Theor. Phys. Suppl. **146**, 388 (2002).

[27] M. Colonna, M. Di Toro, G. Fabbri, and S. Maccarone, Phys. Rev. C **57**, 1410 (1998).

[28] A. B. Larionov, A. S. Botvina, M. Colonna, and M. Di Toro, Nucl. Phys. **A658**, 375 (1999).

[29] S. R. Souza, P. Danielewicz, S. Das Gupta, R. Donangelo, W. A. Friedman, W. G. Lynch, W. G. Tan, and M. B. Tsang, Phys. Rev. C **67**, 051602 (2003).

[30] H. M. Xu, W. G. Lynch, C. K. Gelbke, M. B. Tsang, D. J. Fields, M. R. Maier, D. J. Morrissey, T. K. Nayak, J. Pochodzalla, D. G. Sarantites, L. G. Sobotka, M. L. Halbert, and D. C. Hensley, Phys. Rev. C **40**, 186 (1989).

[31] W. P. Tan, S. R. Souza, R. J. Charity, R. Donangelo, W. G. Lynch, and M. B. Tsang Phys. Rev. C **68**, 034609 (2003).

[32] B. Davin, R. T. de Souza, R. Yanez, Y. Larochelle, R. Alfaro, H. S. Xu, A. Alexander, K. Bastin, L. Beaulieu, J. Dorsett, G. Fleener, L. Gelovani, T. Lefort, J. Poehman, R. J. Charity, L. G. Sobotka, J. Elson, A. Wagner, T. X. Liu, X. D. Liu, W. G. Lynch, L. Morris, R. Shomin, W. P. Tan, M. B. Tsang, G. Verde, and J. Yurkon, Nucl. Instrum. Methods Phys. Res. A **473**, 302 (2001).

[33] A. Wagner, W. P. Tan, K. Chalut, R. J. Charity, B. Davin, Y. Larochelle, M. D. Lennek, T. X. Liu, X. D. Liu, W. G. Lynch, A. M. Ramos, R. Shomin, L. G. Sobotka, R. T. de Souza, M. B. Tsang, G. Verde, and H. S. Xu, Nucl. Instrum. Methods Phys. Res. A **456**, 290 (2001).

[34] R. T. De Souza, N. Carlin, Y. D. Kim, J. Ottarson, L. Phair, D. R. Bowman, C. K. Gelbke, W. G. Gong, W. G. Lynch, R. A. Pelak, T. Peterson, G. Poggi, M. B. Tsang, and H. M. Xu, Nucl. Instrum. Methods Phys. Res. A **295**, 109 (1990); D. W. Stracener, D. G. Sarantites, L. G. Sobotka, J. Elson, J. T. Hood, Z. Majka, V. Abenante, A. ChbihiD, and C. Hensle, *ibid.* **294**, 485 (1990).

[35] L. Phair, D. R. Bowman, C. K. Gelbke, W. G. Gong, Y. D. Kim, M. A. Lisa, W. G. Lynch, G. F. Peaslee, R. T. de Souza, M. B. Tsang, and F. Zhu, Nucl. Phys. **A548**, 489 (1992) and references therein.

[36] G. J. Kunde, S. J. Gaff, C. K. Gelbke, T. Glasmacher, M. J. Huang, R. Lemmon, W. G. Lynch, L. Manduci, L. Martin, M. B. Tsang, W. A. Friedman, J. Dempsey, R. J. Charity, L. G. Sobotka, D. K. Agnihotri, B. Djerroud, W. U. Schröder, W. Skulski, J. Tõke, and K. Wyrozebski, Phys. Rev. Lett. **77**, 2897 (1996).

[37] H. S. Xu, M. B. Tsang, T. X. Liu, X. D. Liu, W. G. Lynch, W. P. Tan, A. Vander Molen, G. Verde, A. Wagner, H. F. Xi, C. K. Gelbke, L. Beaulieu, B. Davin, Y. Larochelle, T. Lefort, R. T. de Souza, R. Yanez, V. E. Viola, R. J. Charity, and L. G. Sobotka, Phys. Rev. Lett. **85**, 716 (2000).

[38] M. B. Tsang, C. K. Gelbke, X. D. Liu, W. G. Lynch, W. P. Tan, G. Verde, H. S. Xu, W. A. Friedman, R. Donangelo, S. R. Souza, C. B. Das, S. Das Gupta, and D. Zhabinsky, Phys. Rev. C **64**, 054615 (2001).

[39] M. Prakash, T. L. Ainsworth, and J. M. Lattimer, Phys. Rev. Lett. **61**, 2518 (1988).

[40] A. Guarnera, M. Colonna, and P. Chomaz, Phys. Lett. B **373**, 267 (1996); A. Guarnera, Thesis, University of Caen, 1996.

[41] M. Di Toro, V. Baran, M. Colonna, S. Maccarone, M. Zielinska-Pfabe, and H. H. Wolter, Nucl. Phys. **A681**, 426c (2001).

[42] V. Baran, M. Colonna, M. Di Toro, and V. Greco, Phys. Rev. Lett. **86**, 4492 (2001).

[43] R. J. Charity, M. A. McMahan, G. J. Wozniak, R. J. McDonald, L. G. Moretto, D. G. Sarantites, L. G. Sobotka, G. Guarino, A. Pantaleo, L. Fiore, A. Gobbi, and K. D. Hildenbrand, Nucl. Phys. **A483**, 371 (1988).

[44] M. B. Tsang, P. Danielewicz, D. R. Bowman, N. Carlin, C. K. Gelbke, W. G. Gong, Y. D. Kim, W. G. Lynch, L. Phair, R. T. de Souza, and F. Zhu, Phys. Lett. B **297**, 243 (1992).

[45] P. Danielewicz and G. F. Bertsch, Nucl. Phys. **A533**, 712 (1991).

[46] H. Feldmeier, K. Bieler, and J. Schnack, Nucl. Phys. **A586**, 493 (1995),

[47] A. Ono, H. Horiuchi, T. Maruyama, and A. Ohnishi, Phys. Rev. Lett. **68**, 2898 (1992); A. Ono and H. Horiuchi, Phys. Rev. C **53**, 2958 (1996).

[48] One might imagine that the fragment isobaric distributions might display a Gaussian dependence on asymmetry, i.e., $Y(N,Z)=f(A)\exp[-(\delta-\bar{\delta})^2/2\sigma^2]$, where $\delta=(N-Z)/A$ and $\bar{\delta}=\langle\delta\rangle$ but we lack the statistics in our simulations to test this hypothesis.

[49] L. G. Sobotka, J. F. Dempsey, R. J. Charity, and P. Danielewicz, Phys. Rev. C **55**, 2109 (1997).

[50] L. Shi and P. Danielewicz, Europhys. Lett. **51**, 34 (2000).

[51] J. F. Dempsey, R. J. Charity, L. G. Sobotka, G. J. Kunde, S. Gaff, C. K. Gelbke, T. Glasmacher, M. J. Huang, R. C. Lemmon, W. G. Lynch, L. Manduci, L. Martin, M. B. Tsang, D. K. Agnihotri, B. Djerroud, W. U. Schröder, W. Skulski, J. Tõke, W. A. Friedman, Phys. Rev. C **54**, 1710 (1996), and references therein.

[52] T. X. Liu *et al.* (unpublished).